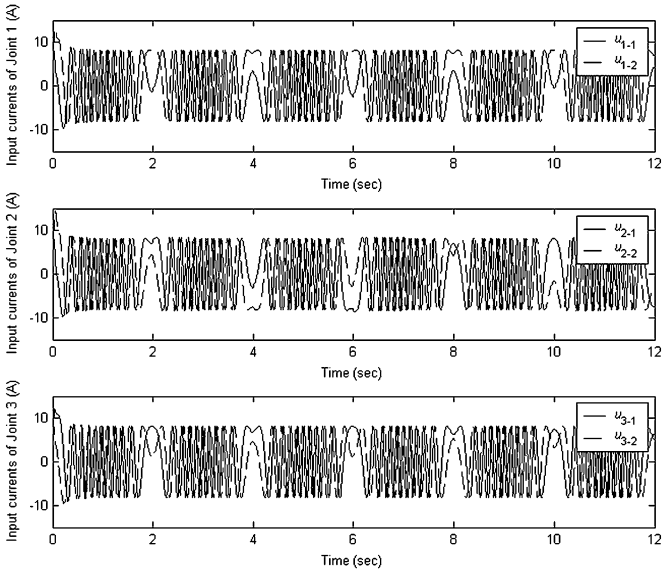

Fig. 2. Current inputs.

$q_3(0) = \pi/2$ (rad), and $\dot{q}_i(0) = 0$ (rad/s), $\psi_{i\_j}(0) = 0$ (wb), $i \in \{1, 2, 3\}, j \in \{2, 3\}$. The value of design parameters was shown in Table I. The initial conditions of the adaptive decentralized control scheme were $\hat{\psi}_{i\_j}(0) = 1$ (wb), $\hat{\theta}_{i\_1}(0) = 1, \hat{a}_i(0) = 11, \hat{m}_i(0) = 0.095, \eta_i(0) = 5, \varepsilon_i(0) = 0.5, i \in \{1, 2, 3\}$, and $j \in \{1, 2\}$. Fig. 1 indicates that all of the tracking errors converge to a residual set, centered at the origin. Fig. 2 displays that all the currents inputs are bounded.

V. Conclusion

This paper proposed an adaptive decentralized control scheme with a rotor-flux observer for tracking control of robot manipulators actuated by current-fed induction motors was proposed. Due to the decentralized manner, it can be implemented with simple hardware. To handle parametric uncertainty in the electromechanical systems, an adaptive law was designed such that all of the signals are bounded and the tracking errors of position, velocity, and rotor fluxes converge to a residual set, centered at the origin, whose size can be reduced by using proper value of design parameters. A satisfactory numerical study of a robot, PUMA 560, driven by current-fed induction motors was provided to verify the effectiveness of the proposed scheme.

References

[1] B. Armstrong, O. Khatib, and J. Burdick, "The explicit dynamic model and inertial parameters of the PUMA 560 arm," in *Proc. IEEE Int. Conf. Robot. Autom.*, 1986, pp. 510–518.

[2] M. Bodson, J. Chiasson, and R. Novotnak, "High-performance induction motor control via input-output linearization," *IEEE Control Syst. Mag.*, vol. 14, no. 4, pp. 25–33, 1994.

[3] P. I. Corke and B. Armstrong-Helouvry, "A search for consensus among model parameters reported for the PUMA 560 Robot," in *Proc. IEEE Int. Conf. Robot. Autom.*, 1994, pp. 1608–1613.

[4] G. Guerrero-Ramírez and Y. Tang, "Decentralized control of rigid robots driven by current-fed induction motor," *J. Dyn. Syst. Meas. Control*, vol. 124, no. 4, pp. 549–553, 2002.

[5] S.-H. Hsu and L.-C. Fu, "Globally fully adaptive decentralized control of robot manipulators," in *Proc. IEEE Int. Conf. Decision and Control*, 2002, pp. 1733–1738.

[6] A.-M. Lee, L.-C. Fu, C.-Y. Tsai, and Y.-C. Lin, "Nonlinear adaptive speed and torque control of induction motors with unknown rotor resistance," *IEEE Trans. Ind. Electron.*, vol. 48, no. 2, pp. 391–401, Apr. 2001.

[7] Y.-C. Lin, L.-C. Fu, and C.-Y. Tsai, "Nonlinear sensorless indirect adaptive speed control of induction motor with unknown rotor resistance and load," *Int. J. Adapt. Control Signal Process.*, vol. 14, pp. 109–140, 2000.

[8] M. W. Spong and M. Vidyasagar, *Robot Dynamics and Control*. New York: Wiley, 1989.

Modeling and Design of Polymer-Based Tunneling Accelerometers by ANSYS/MATLAB

Wei Xue, Jing Wang, and Tianhong Cui

***Abstract*—A prototype design of an inexpensive polymer-based tunneling accelerometer is described in this paper. Instead of silicon, polymethyl methacrylate (PMMA) is used as the mechanical material. By using silicon molds fabricated by conventional lithography and wet-etching techniques in hot embossing, PMMA structures can be replicated within 20 min. The performance of the tunneling sensor can be estimated and improved based on mechanical-level analysis by ANSYS and system-level analysis by MATLAB. The nonlinear tunneling mechanism and electrostatic actuation are linearized using small-signal approximation. To enhance the stability and broaden the bandwidth of the tunneling accelerometer system, a feedback control system with one zero and two poles is designed. The dynamic range of the system is greatly enhanced. The bandwidth of the closed-loop system is approximately 15 kHz.**

***Index Terms*—Feedback control system, hot embossing, polymer, tunneling accelerometer.**

I. Introduction

Electron tunneling effect has been extensively investigated, developed, and used in many applications, since Binning and Rohrer were awarded the Nobel Prize for their original design of the scanning tunneling microscope (STM) in 1986 [1]–[4]. High-performance accelerometers are in great demand in many applications such as acoustic measurement, seismology, and navigation. Considerable research work on accelerometers has been reported by several groups [5]–[8]. Compared to other common and well-developed accelerometers such as capacitive, piezoresistive, piezoelectric accelerometers, tunneling accelerometers may easily achieve higher sensitivity and higher resolution with smaller size due to the exponential relationship between the tunneling current and the tunneling gap. However, tunneling sensors are usually more difficult to be fabricated than others. Since tunneling current can only be observed when the gap between the tunneling tip electrode and its counter electrode is in the range of 10 Å, tunneling sensors normally operate in closed-loop mode. Several models and systems were developed for tunneling accelerometers [6]–[8].

Polymer-based microelectromechanical systems (MEMS) have gained a broad theoretical interest and practical applications in the past 10 years [9]–[13]. Polymers offer many advantages for sensor technology. They are low cost, flexible, chemically and biologically compatible, and easy to be processed. Polymer microsensors are becoming more and more important, and can be low-cost alternatives to the silicon-based or glass-based microsensors.

Manuscript received July 27, 2004; revised March 17, 2005 and April 20, 2005. Recommended by Technical Editor I.-M. Chen. This work was supported in part by Grants NSF/LEQSF (2001-04)-RII-02, DARPA DAAD19-02-1-0338, and by NASA (2002)-Stennis-22.

The authors are with the Department of Mechanical Engineering University of Minnesota, Minneapolis, MN 55455 USA (e-mail: tcui@me.umn.edu).

Digital Object Identifier 10.1109/TMECH.2005.852451

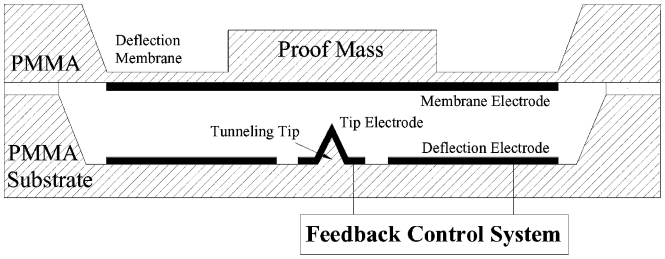

Fig. 1. Schematic diagram of a polymer-based tunneling accelerometer.

Our objective is to design and fabricate polymer-based tunneling accelerometers. Polymethyl methacrylate(PMMA) is used as the mechanical material. Hot embossing technique is used to transfer the patterns from the silicon molds to PMMA. Since new polymer material is used, simulation works can be helpful to estimate the static and dynamic properties of the device. ANSYS and MATLAB are utilized as the computer-aided tools to make mechanical and system-level analyses, which can benefit the design and development of the tunneling accelerometer. Based on finite element model (FEM) and a linearized mathematical model, the mechanical properties, performance, stability, responsibility, and dynamic range of the system can be estimated. In addition, the fabrication and the measurement of the device are briefly introduced.

II. Sensor Structure and Fabrication

To explore the tunneling sensor technology, polymers, and hot embossing technique, all polymer-based vertical tunneling accelerometers have been developed in our lab. As shown in Fig. 1, a typical tunneling accelerometer consists of two mechanical components and three gold electrodes. The mechanical components comprise a substrate with a tunneling tip and a membrane with a proof mass. The electrodes include a tunneling tip electrode, a membrane electrode, and a deflection electrode. By applying a high-deflection voltage on the bottom deflection electrode, the electrostatic force attracting the top membrane to bend downward can be established, and the tunneling gap can be controlled. The tunneling current can be generated when the gap between the tunneling tip and its counter electrode is in the range of 10 Å, and the current will remain constant if the gap keeps unchanged. In the low bias region, the tunneling current I_t is linearly proportional to the applied junction bias V_B, and exponentially proportional to the distance of the tunneling gap.

Instead of silicon, an amorphous polymer material, PMMA (Cyro Industries ROHAGLAS 99530), is chosen as the mechanical material. Hot embossing technique is used to fabricate all the PMMA mechanical microstructures. PMMA has unique thermal and mechanical properties which make it behave ideally in hot embossing process. The glass transition temperature T_g and the melting temperature T_m of the PMMA are 98 °C and 170 °C, respectively. By using well-developed silicon molds with sharp angles and smooth surfaces, the PMMA structures can be easily replicated within 20 min [14]. The silicon molds are fabricated using conventional silicon bulk-micromachining techniques, as shown in Fig. 2(a)–(e). The fabrication process for the PMMA structures using hot embossing is shown in Fig. 2(f)–(h). The silicon mold was lowered to such an extent that it just touched the surface [see Fig. 2(f)]. The mold and PMMA were heated at the same time above T_g to ensure sufficient flow ability of the PMMA. The silicon mold was pressed into the PMMA under a controlled force [see Fig. 2(g)]. After filling the microcavities of the silicon mold, the PMMA was cooled down and the patterned PMMA was demolded [see Fig. 2(h)]. Fig. 3 shows a replicated PMMA pyramid tip with smooth surfaces, sharp tip point, and steep edges.

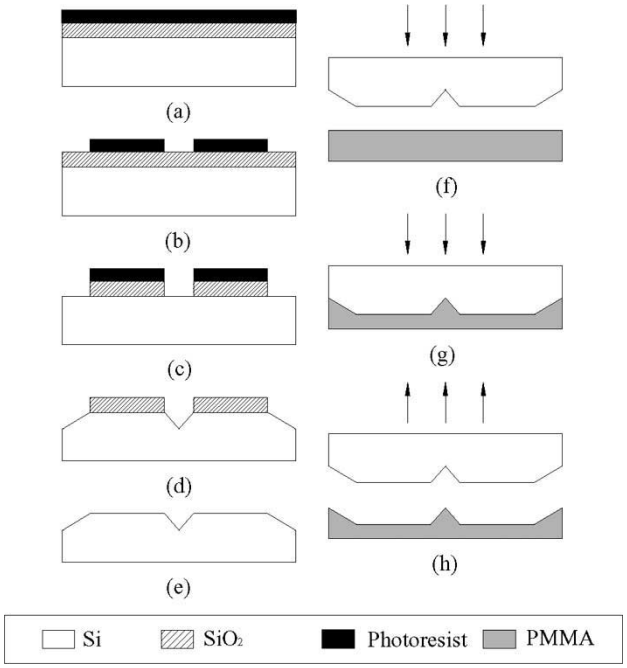

Fig. 2. Fabrication process of silicon mold and PMMA structure.

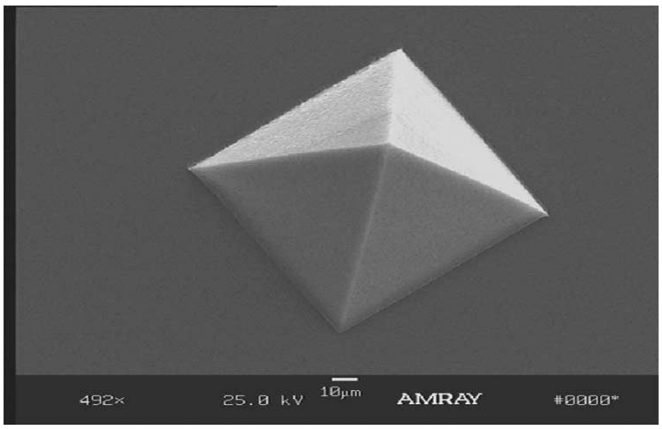

Fig. 3. SEM image of a PMMA pyramid tip fabricated by hot embossing.

III. Mechanical-Level Analysis

ANSYS, an engineering package for general purpose finite element analysis, is used to simulate the mechanical properties of the device. A number of structures have been simulated by ANSYS. A square-shaped membrane structure (4×4 mm $\times$ 30 μm) without proof mass is described here for its simplicity. ANSYS is helpful in handling complex structures, which are difficult to calculate analytically.

The spring constant of the membrane, with all edges fixed, can be expressed as [15]:

$$k = \frac{E \cdot t^3}{\alpha \cdot l^2} \tag{1}$$

where E is the Young's Modulus of PMMA (2 GPa), $\alpha = 0.0135$, $t = 30$ μm, and $l = 4$ mm. Therefore, the spring constant k is 250 N/m. By static analysis, the displacement of the membrane can be estimated by ANSYS, and the corresponding spring constant k can be calculated as

276 N/m. The difference between the simulated result and the calculated result comes from the high-aspect-ratio membrane structure. Compared with silicon, PMMA is "soft" material. The Young's Moduli of PMMA and silicon are 2 GPa and 165 GPa, respectively. From (1), the spring constant of membrane is proportional to E and t^3. For structures with same dimension, the spring constant of PMMA is much smaller than silicon. In other words, to obtain the same spring constant, a PMMA-based structure can be much thicker than a silicon-based structure. This will benefit the design and the fabrication process.

Modal analysis and Harmonic analysis are used to determine the frequency response of the membrane structure. Damping ratio is required in the analysis. In air environment, the damping coefficient of the membrane can be calculated as $b = 1.96 \times 10^{-3}$ Ns/m. The damping ratio is calculated as $\xi = 0.0833$. Therefore, the mechanical quality factor $Q = 0.5/\xi = 6$. As estimated in ANSYS, the membrane has the largest displacement at 4518 Hz, which is very close to the theoretical natural frequency (4462 Hz) of the square-shaped membrane structure.

The static sensitivity of the structure is defined as $S = \Delta z/a = m/k$, where Δz is the maximum displacement of the membrane, and a is the external acceleration applied on the structure surface. The total noise equivalent acceleration (TNEA) of thermal-mechanical noise is given by [2]

$$\text{TNEA} = \sqrt{\frac{4k_B T\omega}{mQ}} \tag{2}$$

where k_B is the Boltzmann constant, T is the temperature, and ω is the natural frequency of the membrane. The static sensitivity of the PMMA membrane is calculated as 22 nm/g; and the TNEA (at room temperature) is 12.8 mg/$\sqrt{}$Hz. For silicon structure with the same dimension, the static sensitivity and the TNEA are approximately 5.3 Å/g, and 5.72 mg/$\sqrt{}$Hz, respectively. Therefore, compared to silicon structures, PMMA structures have much higher static sensitivity but relatively lower resolution. The lower resolution is because of the lower quality factor Q of the PMMA structures.

IV. Mathematical Model and System-Level Analysis

MATLAB is used to build the mathematical model of the tunneling accelerometer. The model is composed of different function blocks based on Laplace transforms. In general, tunneling sensor with the feedback control system is not a linear system. Assumptions and approximations are used to linearize the system.

The membrane is the sensing part of the accelerometer. It can be considered as a suspended mass-spring-damping system [16]. Using Laplace transforms, the dynamic performance of the membrane can be expressed as

$$\frac{\Delta x}{a_{\text{ext}}} = \frac{1}{S^2 + \frac{b}{m}S + \frac{k}{m}} \tag{3}$$

where m, b, and k represent the mass, damping coefficient, and spring constant of the membrane, respectively, a_{ext} is external acceleration, Δx is the center point displacement of the membrane.

For tunneling accelerometers, the tunneling current is exponentially proportional to the change of the tunneling gap, which is given by

$$I = I_0 \cdot \exp(-\alpha\sqrt{\Phi}\Delta x) \tag{4}$$

where I_0 is the operation tunneling current, $\alpha = 1.025$ Å^{-1} eV$^{-0.5}$, Φ is the effective tunneling barrier height or the effective work function of the electrode material, and Δx is the change of the tunneling gap between two electrodes. Since $\Delta x \ll 10$ Å, the tunneling current can be developed by Taylor series as [17]

$$I = I_0(1 - \alpha\sqrt{\Phi}\Delta x) \tag{5}$$

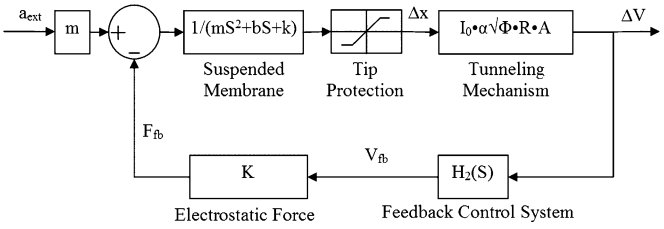

Fig. 4. Mathematical model of the tunneling accelerometer.

TABLE I
Nominal Design Parameters of the Tunneling Accelerometer

Design Parameters	Values
Mass, *m*	552 μg
Spring constant, *k*	276 N/m
Damping coefficient (in air), *b*	1.96×10^{-3} N·s/m
Mechanical quality factor, *Q*	6
Feedback constant, *K*	5.7×10^{-6} N/V

The change of the output voltage ΔV can be presented by

$$\Delta V = (I - I_0) \cdot R \cdot A = I_0 \cdot \alpha\sqrt{\Phi} \cdot R \cdot A \cdot \Delta x \tag{6}$$

where R is the resistance of a high value resistor, and A is the amplitude of the amplifier. Therefore, based on the small displacement of the membrane, the nonlinear tunneling mechanism can be linearized.

For the actuator, the electrostatic force is proportional to the square of the applied voltage, which is composed of a dc constant voltage V_{dc} and the feedback voltage V_{fb}. Since V_{dc} ($\sim$100 V) is much higher than V_{fb} (several millivolts), the electrostatic force can be given by

$$F_{\text{es}} \propto V_a^2 = (V_{\text{dc}} + V_{\text{fb}})^2 \approx V_{\text{dc}}^2 + 2V_{\text{dc}}V_{\text{fb}}. \tag{7}$$

The first item is used to set the operation point, and the second item is related to the feedback force applied to the membrane. The feedback force can be simplified as

$$F_{\text{fb}} = K \cdot V_{\text{fb}} \tag{8}$$

where K is the feedback constant. A possible value of K is 5.7×10^{-6} N/V with an overlapped area of 4 $\times$ 4 mm, a nominal gap of 50 μm, and a high dc voltage of 100 V.

Based on all the approximations above, the whole system can be linearized and modeled. The detailed function block diagram is shown in Fig. 4. The transfer function of the whole system can be expressed as

$$\frac{\Delta V}{a} = \frac{m \cdot H_1(S)}{1 + K \cdot H_1(S)H_2(S)} = \frac{m \cdot I_0 \cdot \alpha\sqrt{\Phi} \cdot RA}{(mS^2 + bS + k) + \cdot K \cdot I_0 \cdot \alpha\sqrt{\Phi} \cdot RA \cdot H_2(S)} \tag{9}$$

$H_1(S)$ represents the mechanism of the suspended membrane/proof mass and the electron tunneling mechanism. $H_2(S)$ is the feedback control system to transfer the output voltage ΔV to the feedback voltage V_{fb}, which can be optimized by MATLAB simulation. The objective of this feedback control system is to enhance the system stability and responsibility while broadening the bandwidth.

Based on the linearized model, the system can be simulated and the characteristics of the tunneling accelerometer can be evaluated. Table I lists the nominal design parameters of the tunneling accelerometer. $H_1(S)$ has two complex poles at $-1.78 \times 10^3 \pm j \cdot 2.23 \times 10^4$. To

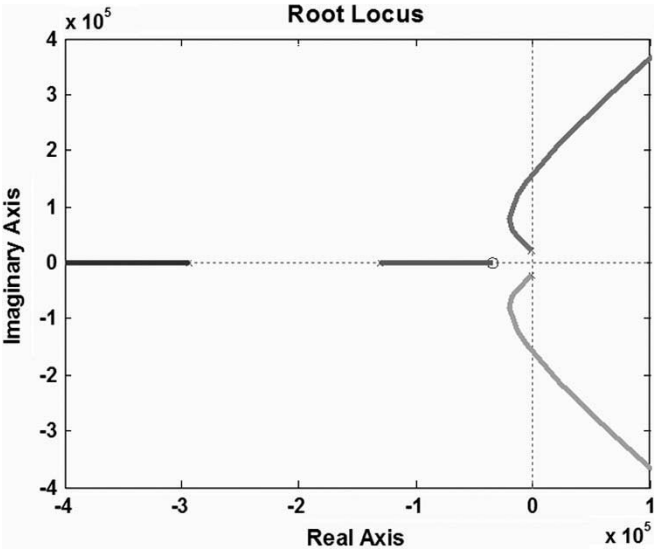

Fig. 5. Root locus of the tunneling accelerometer system.

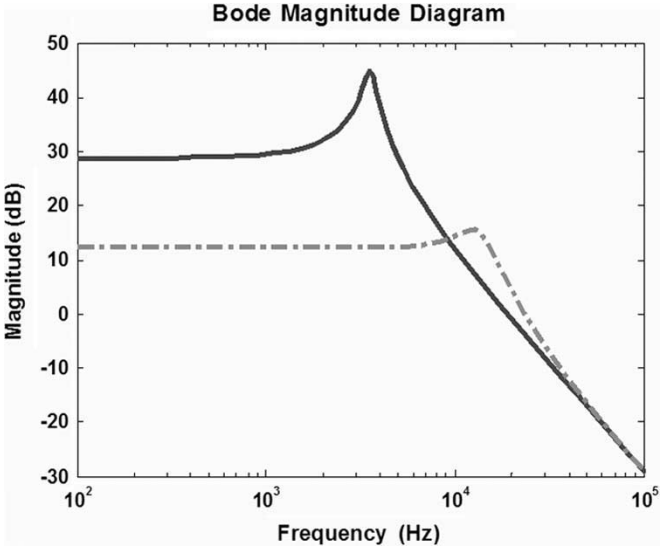

Fig. 6. Magnitude frequency response of the open-loop and closed-loop accelerometer systems.

meet the requirements of the system stability, time responsibility, and bandwidth, there are infinite numbers of $H_2(S)$ can be used. In order to simplify the system, a well designed transfer function $H_2(S)$ with one zero and two poles is enough to meet the requirements. The feedback control system $H_2(S)$ is designed to have one zero at -3.4×10^4, and two poles at -2.9×10^5 and -1.3×10^5. $H_2(S)$ can be easily realized by a simple circuit using several electronic components such as resistors, capacitors, and amplifiers, etc.

The stability of the accelerometer system can be predicted by checking its root locus. Root locus is a powerful graphic method to determine the poles of a closed-loop system. For a stable system, all the poles are required to stay on the left side of the s-plane. The root locus of the system is shown in Fig. 5. All the poles can locate on the left side of the s-plane by adjusting the loop gain. The step response analysis of the closed-loop system shows that the settling time can be less than 0.25 ms.

To maintain the constant tunneling current, tunneling accelerometers are operated in closed-loop mode. The bandwidth of the system can be extended due to the feedback control system. The sensitivity magnitude frequency responses of the open-loop (solid line) and the closed-loop (dashed line) systems are plotted in Fig. 6. Though the sensitivity of the closed-loop system is decreased in the low frequency region, the dynamic range of the system is greatly enhanced. The bandwidth of the closed-loop accelerometer system is approximately 15 kHz.

V. Measurement

After assembling of the polymer sensor, the frequency response of the membrane can be easily measured. The membrane electrode is connected to ground and an ac voltage (with amplitude 7 V) is applied on the deflection electrode. Therefore, electrostatic force is generated between two electrodes. The membrane will oscillate due to the applied force. A laser interferometer is used to detect the small displacement of the membrane. The open-loop frequency response of the sensor is shown in Fig. 7. The natural frequency of the polymer sensor is approximately 4500 Hz, and the highest displacement is 260 nm. The displacement amplitude is higher than 210 nm at frequencies up to 5500 Hz. The value of the natural frequency and the shape of the plot are close to the simulation result of the open-loop system as shown in Fig. 6.

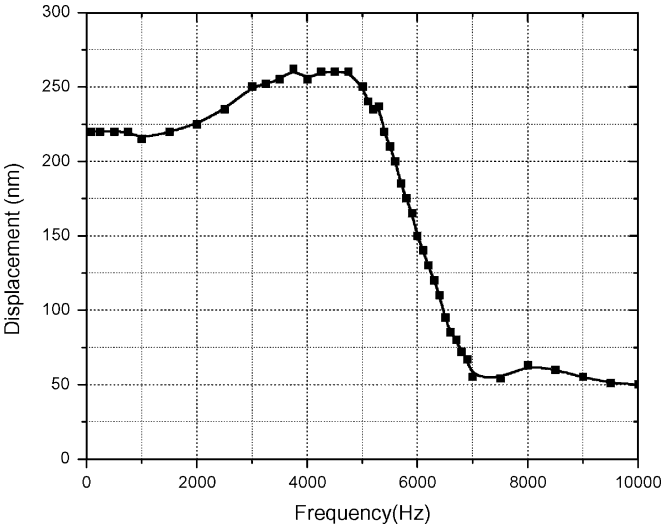

Fig. 7. Open-loop frequency response of the polymer structure.

VI. Conclusion

In this brief, modeling and design of polymer-based tunneling accelerometers are described. ANSYS is used for mechanical-level analysis. Mechanical properties and frequency response of the structure can be obtained from the simulation results. For a simple membrane structure with dimension of 4×4 mm$\times 30$ μm, the static sensitivity and the resolution can be calculated as 22 nm/g and 12.8 mg/$\sqrt{}$Hz, respectively. MATLAB is used for the system-level analysis. A simple but effective mathematic model is built. Based on small signal variation of the sensor, the system can be linearized. A feedback control system with one zero and two poles can stabilize the system and broaden the bandwidth. Simulation results including root locus, step response, open-loop and closed-loop frequency responses are described and discussed. Frequency response of a polymer accelerometer is shown in the paper. The value of the natural frequency and the shape of the plot are close to the simulation results.

REFERENCES

[1] G. Binning, H. Rohrer, Ch. Gerber, and E. Weibel, "Surface studies by scanning tunneling microscopy," *Phys. Rev. Lett.*, vol. 49, pp. 57–61, 1982.

[2] C. H. Liu and T. W. Kenny, "A high-precision, wide-bandwidth micromachined tunneling accelerometer," *J. Microelectromech. Syst.*, vol. 10, no. 3, pp. 425–433, Sep. 2001.

[3] T. W. Kenny, J. K. Reynolds, J. A. Podosek, E. C. Vote, L. M. Miller, H. K. Rockstad, and W. J. Kaiser, "Micromachined infrared sensors using tunneling displacement transducers," *Rev. Sci. Instrum.*, vol. 67, no. 1, pp. 112–128, 1996.

[4] R. L. Kubena, D. J. Vickers-Kirby, R. J. Joyce, F. P. Stratton, and D. T. Chang, "New tunneling-based sensor for inertial rotation rate measurements," *Sens. Actuators A, Phys.*, vol. 83, no. 1, pp. 109–117, 2000.

[5] C. H. Liu, A. M. Barzilai, J. K. Reynolds, A. Patridge, T. W. Kenny, J. D. Grade, and H. K. Rockstad, "Characterization of a high-sensitivity micromachined tunneling accelerometer with micro-g resolution," *J. Microelectromech. Syst.*, vol. 7, no. 2, pp. 235–244, Jun. 1998.

[6] C. Yeh and K. Najafi, "CMOS interface circuity for a low-voltage micromachined tunneling accelerometer," *J. Microelectromech. Syst.*, vol. 7, no. 1, pp. 6–15, Mar. 1998.

[7] C. H. Liu, H. K. Rockstad, and T. W. Kenny, "Robust controller design via μ-synthesis for high-performance micromachined tunneling accelerometers," in *Proc. 1999 American Control*, San Diego, CA, 1999, pp. 247–252.

[8] A. Partidge, J. K. Reynolds, J. D. Grade, B. J. Kane, N. I. Maluf, G. T. A. Kovacs, and T. W. Kenny, "Integrated controller for tunnel sensors," *IEEE J. Solid-State Circuits*, vol. 34, no. 8, pp. 1099–1107, Aug. 1999.

[9] H. Becker and U. Heim, "Hot embossing as a method for the fabrication of polymer high aspect ratio structures," *Sens. Actuators A, Phys.*, vol. 83, no. 1, pp. 130–135, 2000.

[10] E. W. H. Jager, E. Smela, and O. Inganas, "Microfabricating conjugated polymer actuators," *Science*, vol. 290, no. 5496, pp. 1540–1545, 2000.

[11] G. Harsányi, "Polymer films in sensor applications: A review of present uses and future possibilities," *Sens. Rev.*, vol. 20, no. 2, pp. 98–105, 2000.

[12] M. J. Madou, L. J. Lee, S. Daunert, S. Lai, and C. Shih, "Design and fabrication of CD-like microfluidic platforms for diagnostics: Microfluidic functions," *Biomed. Microdevices*, vol. 3, no. 4, pp. 245–254, 2001.

[13] G. Lee, S. Chen, G. Huang, W. Sung, and Y. Lin, "Microfabricated plastic chips by hot embossing methods and their applications for DNA separation and detection," *Sens. Actuators B, Chem.*, vol. 75, no. 1–2, pp. 142–148, 2001.

[14] J. Wang, W. Xue, and T. Cui, "A combinative technique to fabricate hot embossing master for PMMA tunneling sensors," *Microsyst. Technol.*, vol. 10, no. 4, pp. 329–333, 2004.

[15] W. C. Young, *Roark's Formulas for Stress and Strain*, 6th ed., New York: McGraw-Hill, 1989.

[16] C. P. Lewis, M. Kraft, and T. G. Hesketh, "Mathematical model for a micromachined accelerometer," *T. I. Meas. Control*, vol. 18, no. 2, p. 9298, 1996.

[17] J. Wang, Y. Zhao, T. Cui, and K. Varahramyan, "Synthesis of the modeling and control systems of a tunneling accelerometer using the MatLab simulation," *J. Micromech. Microeng.*, vol. 12, no. 6, pp. 730–735, 2002.